ACS OMEGA

Article

Cite This: ACS Omega 2018, 3, 2735−2742

Fabrication by Laser Irradiation in a Continuous Flow Jet of Carbon Quantum Dots for Fluorescence Imaging

Carlos Doñate-Buendia,*[,†] Rafael Torres-Mendieta,[‡] Alexander Pyatenko,[§] Eva Falomir,[∥] Mercedes Fernández-Alonso,[†] and Gladys Mínguez-Vega*[,†]

[†]GROC·UJI, Institute of New Imaging Technologies, Universitat Jaume I, Avda. Sos Baynat sn, 12071 Castellón, Spain

[‡]Institute for Nanomaterials, Advanced Technologies and Innovation, Technical University of Liberec, Studentská 1402/2, 461 17 Liberec, Czech Republic

[§]Nanomaterials Research Institute, National Institute of Advanced Industrial Science and Technology (AIST), Tsukuba Central 5, 1-1-1 Higashi, Tsukuba, Ibaraki 305-8565, Japan

[∥]Department of Inorganic and Organic Chemistry, University Jaume I, Avda. Sos Baynat sn, 12071 Castellón, Spain

Supporting Information

ABSTRACT: Fluorescent carbon quantum dots (CQDs) are synthesized by laser irradiation of carbon glassy particles suspended in polyethylene glycol 200 by two methods, a batch and a flow jet configuration. The flow jet configuration is carried out by the simple combination of common laboratory objects to construct a home-made passage reactor of continuous flow. Despite the simplicity of the system, the laser energy is better harvested by the carbon microparticles, improving the fabrication efficiency a 15% and enhancing the fluorescence of CQDs by an order of magnitude in comparison with the conventional batch. The flow jet-synthesized CQDs have a mean size of 3 nm and are used for fluorescent imaging of transparent healthy and cancer epithelial human cells. Complete internalization is observed with a short incubation time of 10 min without using any extra additive or processing of the cell culture. The CQDs are well fixed in the organelles of the cell even after its death; hence, this is a simple manner to keep the cell information for prolonged periods of time. Moreover, the integrated photostability of the CQDs internalized in in vitro cells is measured and it remains almost constant during at least 2 h, revealing their outstanding performance as fluorescent labels.

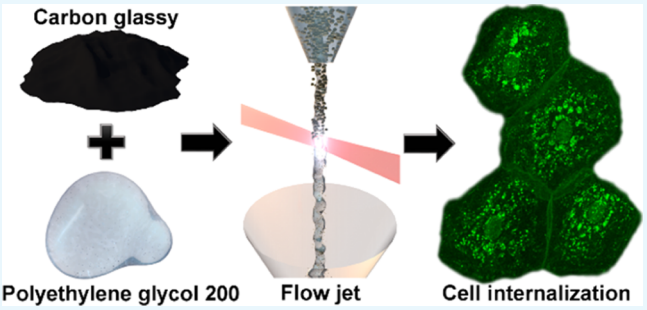

INTRODUCTION

Fluorescence carbon quantum dots (CQDs) are described as carbon nanoparticles of less than 10 nm diameter that demonstrate a fluorescence emission. In spite of being discovered at the beginning of the 21st century,[1] in a short period of time, CQDs have emerged as a powerful low toxic, environmentally friendly, and low-cost nanomaterial with promising perspectives. Their impact in the nanotechnology community has had a direct and remarkable influence on applications such as in vivo imaging,[2] cancer therapy,[3] biosensing,[4] and solar energy conversion.[5] Among the vast majority of the available nanoscopic fluorescent agents, CQDs stand out from the rest because of their outstanding physicochemical properties such as tunable photoluminescence, high photostability against photobleaching and blinking, easy surface passivation and functionalization, and favorable biocompatibility.[6−9]

Stimulated by a rapid growth of research interest in CQDs, numerous chemical and physical synthesis techniques have been developed. Common routes for preparing fluorescent CQDs include collecting the soot of a burning candle,[10] hydrothermal treatment,[11] microwave synthesis,[12] pyrolysis,[13] ultrasonic synthesis,[14] and so forth. Among all of them, laser synthesis has stood out above the rest because it constitutes a single-step, green, and simple strategy that neither requires the use of external chemical agents nor promotes the creation of byproducts that may lead to further cross chemical effects, guarantying in this way a high-purity synthesis of CQDs[15−19] and nanodiamonds.[20,21] The high purity of the manufactured materials makes possible their effective implementation in extremely sensitive systems, such as human being cells[22] or in vivo animals.[23] Principal laser synthesis methods of carbon dots can be classified in laser ablation of carbonaceous solid targets immersed in a liquid[15,16] and laser fragmentation of suspensions containing the powder carbon material.[17−19]

The laser fragmentation in liquids technique is based on the irradiation of a suspension composed of micrometric or nanometric solid particles dispersed in a liquid with a pulsed

Received: December 29, 2017
Accepted: February 23, 2018
Published: March 7, 2018

DOI: 10.1021/acsomega.7b02082
ACS Omega 2018, 3, 2735−2742

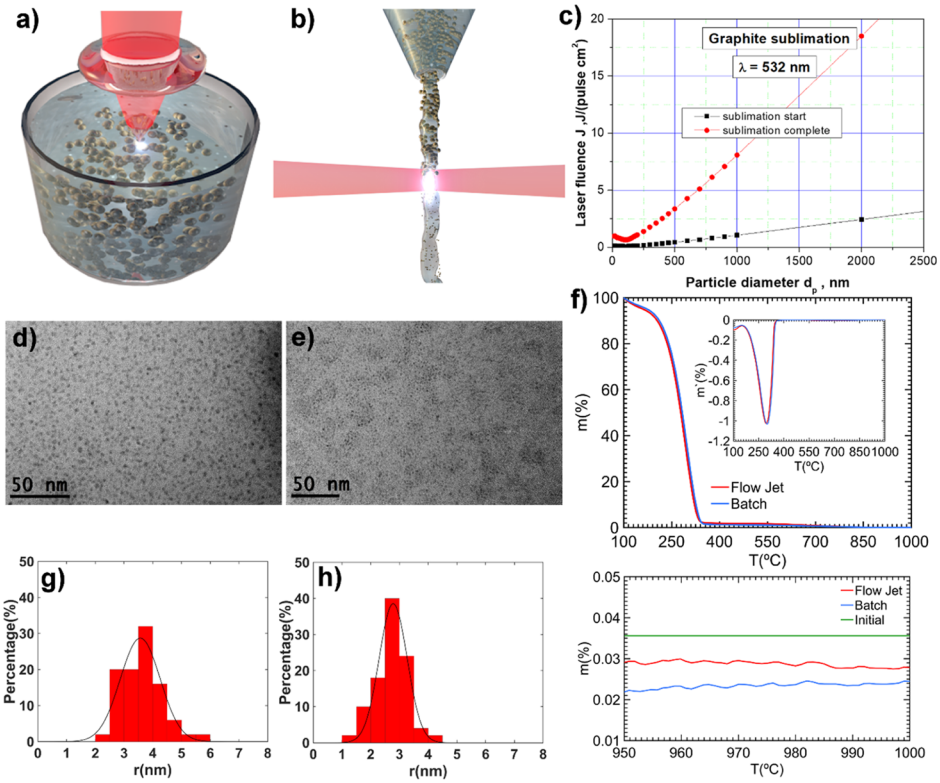

Figure 1. Scheme of laser irradiation of a suspension in (a) typical batch and (b) continuous flow jet setups. (c) Fluences at which graphite particles start to sublimate and sublimate completely. TEM micrographs of the formation of CQDs with (d) typical batch and (e) continuous flow jet (the size distributions are displayed below, respectively (g,h) histograms). (f) TGA of the supernatant of both products is shown in the top, together with the extended residual zone in the bottom.

laser source. The interaction between the intense laser radiation and the colloid leads to the size reduction of the solid content through photothermal vaporization or Coulomb explosion mechanisms, depending on the laser fluence and pulse duration,[24−28] leading to an exceptional accuracy in reshaping.[29] In a conventional batch processing configuration, shown in Figure 1a, the powder carbon material is dispersed into the solvent and the suspension is contained in a glass cell for laser irradiation. During irradiation, a magnetic stirrer or ultrasound is used to expedite the movement of carbon particles and prevent gravitational settling. Although this procedure to synthesize carbon dots has provided excellent results, it also presents some disadvantages. On the one hand, graphite or carbon nanoparticles lead to the production of a black suspension so the laser beam experiences a fluence gradient within the irradiated volume because of the losses by scattering or absorption. This fact causes a reduced control of the process as different mechanisms such as fragmentation and melting may occur simultaneously in the vessel. On the other hand, as the total liquid volume is larger than the irradiated volume, the method does not guarantee that all the particles pass through the laser beam; hence, there is a mixing of the synthesized material and leftovers that should be removed by postprocessing treatment to get rid of the bigger carbonaceous material by centrifugation or other methodologies. To the best of our knowledge, an alternative synthesis method using the flow jet passage reactor has never been explored to synthesize CQDs. In this method, first proposed in 2010 by Wagener and Barcikowski, the laser beam is focused in a thin liquid jet composed of microparticles in suspension (see Figure 1b).[30] Then, the solid content suspended in the liquid is being irradiated at the same fluence, promoting the same processing conditions for the entire sample and a more efficient energy delivery of laser radiation.[31,32]

In this research, we use a low-cost liquid jet passage reactor (see Figure S1) in the continuous operation mode to synthesize CQDs. A comparative study with a batch processing configuration demonstrates that the flow jet has higher production efficiency and an enhanced fluorescent response, and it is the most appropriate method toward a scale-up synthesis of CQDs with laser. Once the superior performance of the CQDs synthesized by the passage reactor is proved, the nanoparticles are used as in vivo biomarkers in sane and cancer human being cells with long-term photostability even in degraded cells.

RESULTS AND DISCUSSION

The irradiated colloid is an 11 mL sample taken from an initial sample of 40 mg of carbon glassy particles dispersed in 100 mL of polyethylene glycol 200 (both purchased from Sigma-Aldrich). The original size of carbon solid particles is 2−12 μm, but the suspension was milled till most of the particles got a size of around 1 μm (images of the size distribution of the nanoparticles measured by dynamic light scattering are provided in Figure S2, Supporting Information). The laser irradiation was carried out using the second harmonic of a Nd:YAG pulsed laser (Brilliant, Quantel), with a pulse width of 4 ns Full Width at Half Maximum (fwhm) at a fundamental wavelength of 1064 nm and a repetition rate of 10 Hz. The laser radiation power over the suspension was set to 300 mW at 532 nm. It was focused by a cylindrical lens with a focal length of 300 mm, providing a fluence of ~6 J/cm^2 at the focal spot. In

DOI: 10.1021/acsomega.7b02082
ACS Omega 2018, 3, 2735−2742

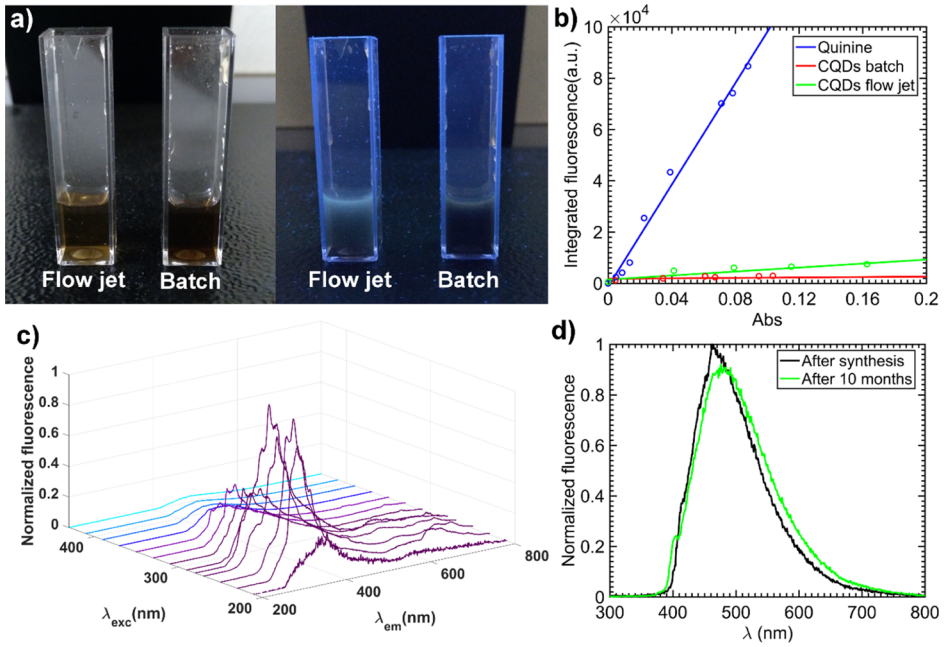

Figure 2. (a) Aspect of both samples under natural illumination, left, and after being illuminated with 365 nm UV light, right. The photoluminescence is higher for the flow jet sample, which can be observed by the naked eye. (b) Linear fits of the integrated fluorescence intensities against the absorbance obtained from the reference fluorophore and the two samples for the measurement of their QY. (c) Broadband emission photoluminescence spectra of the CQDs synthesized with the continuous flow jet. (d) Photoluminescence response for 405 nm excitation light for a sample after generation and a sample stored for 10 months.

batch processing, the focal spot was located 2 mm inside the cuvette containing the educt, and the liquid was constantly stirred by means of a magnetic stirrer at 100 rpm. In the flow jet, the focal spot size in the direction of liquid flowing is 4 mm to irradiate the maximum number of particles; this guarantees that the particles are reached mostly by the same laser fluence. The period of flux in the liquid jet flow was 30 s. Further details of the fabrication of a low-cost continuous flow jet and a short video (Video S1) of the experimental setups can be found in Supporting Information section S1.

The appropriate fluence for laser fragmentation was determined through a modification of the particle heating–melting–evaporation model.[24,33] As there is not enough reliable thermodynamic data and absorption characteristics for the black carbon material dispersed in PEG, all estimations were made for graphite particles of the same sizes.[34,35] However, as the graphite never melts but experiences sublimation at high temperatures, the original model was modified to estimate the critical fluence values at which particles start to sublimate and sublimate completely, see Figure 1c. Details of the theoretical calculations can be found in Supporting Information section S3. The fluence value of 6 J/cm^2 for the irradiation is chosen to assure a complete sublimation process even for bigger particles. Even though it can be seen in Figure 1c that for carbon black particles of 1 μm(initial irradiation particle size shown in Figure S2, Supporting Information) the fluence value needed for complete sublimation is about 8 J/cm^2, for 6 J/cm^2, the sublimation process is initiated and after several irradiation cycles, the particles are effectively reduced to CQDs. The value of 6 J/cm^2 is experimentally found to be the optimum for our system. Higher fluence values lead to the generation of nonlinear effects in the liquid jet as well as instabilities of the flow jet. Lower fluence values increase the necessary number of cycles for particle size reduction, besides, big particles can even be not reduced if the fluence value is lower than the sublimation start value for that particle size (Figure 1c).

The flow jet solution changed its color progressively from gray to caramel color after ∼3 h of laser irradiation, which indicated the formation of CQDs (see the complete evolution in Figure S3). As the batch-processing sample showed a darker brown, the processing time of both samples was set to 4 h. Transmission electron microscopy (TEM) micrographs displayed in Figure 1d,e show the characteristic spherical morphology of laser-synthesized CQDs. In batch processing, the average size of the CQDs obtained by Gaussian fitting of the size distribution, Figure 1g, is (3.57 ± 0.07) nm with a curve width of 0.49 nm. In the flow jet, the average size measured, Figure 1h, is (2.78 ± 0.04) nm and a width of 0.34 nm. Both techniques lead to a similar size reduction, but by using the flow jet technique, it is possible to reduce the material in a more effective way due to the fact that laser fluence can be delivered to the particles in a more efficient way. The improved control over the fluence in the irradiation achieved by the flow jet system also reduces size dispersion of the CQDs obtained as well as the amount of big particles in the final sample (Figure S4, Supporting Information). Moreover, for a period of observation of 10 months, no changes were observed in color, size, stability, or properties of the CQDs (see Figures 2d and S8, Supporting Information). Their long-term stability proves the generated CQDs as an excellent option for bionanotechnology-related applications.

Thermogravimetric analysis (TGA) of the supernatant of both products after undergoing centrifugation for 30 min at 4000 rpm (Figure 1f) revealed that the use of the flow jet strategy leads to the manufacture of the highest amount of CQDs, where (83.9 ± 0.2)% of the original solid content is turned into useful CQDs, with a final concentration of CQDs being 0.029 wt %, whereas the classical strategy only leads to the reduction of (68.7 ± 1.3)% of the original amount, with a

DOI: 10.1021/acsomega.7b02082
ACS Omega 2018, 3, 2735−2742

final concentration of CQDs being 0.023 wt % (details of the calculation can be found in Supporting Information section S2).

As lasers are easily integrated in a production chain, it is interesting to automate the process of synthesis of CQDs, as the methods proposed up to now are discontinuous in time. The obtained results are a proof-of-concept that proves that the passage reactor can provide a good strategy to achieve a continuous, high quality, and high production process for the synthesis of CQDs without the necessity of replacing a solid target or a liquid suspension in short periods of time. In this sense, it is envisioned as a suitable method for laser synthesis of CQDs for industrial production.

Expected visible photoluminescence was observed in the prepared samples according to the reduced size of the CQDs generated. To confirm that the fluorescence was emitted from the CQDs and not from the liquid solvent, the PEG200 was irradiated by a 405 nm laser pointer showing a mild emission (see Figure S5, Supporting Information). Interestingly, it is clearly seen by the naked eye that when the samples are illuminated with 365 nm UV light, the photoluminescence is higher for the flow jet samples (Figure 2a), which is confirmed by measuring the quantum yield (QY) (Figure 2b). On the basis of the comparative method,[36] the QY is calculated using the slope of the line determined from the plot of the integrated fluorescence intensities against the absorbance. In this case, the QY can be calculated as $QY = Q_r(m/m_r)(n/n_r)$,[2] where m stands for the slope of the line and n is the refractive index of solvent. The subscript r represents the reference fluorophore of known QY; quinine sulfate (in 0.1 M H_2SO_4) was used in this case. The resulting linear fits obtained from the reference fluorophore and the two samples are shown in Figure 2b. These results show that the QY of the CQDs synthesized with the flow jet (4.5%) is approximately 1 order of magnitude higher than the ones obtained with the batch system (0.5%).

It should be noted that the samples obtained with the batch and the flow jet setups are prepared from the same initial suspension of carbon black microparticles, and hence the concentration of carbon is the same in every sample and does not affect the QY measurements. The color differences are due to the reduced efficiency of the batch configuration in reducing particle size, 15% higher efficiency for the flow jet configuration. This fact can be clearly seen in Figure S8; after 10 months, the particles that are not reduced to CQDs sedimentate and the color of both samples gets similar. Inspection of TEM pictures (Figure S4, Supporting Information) prove the presence of a larger population of micrometric carbon pieces for the batch resulting in a darker color for the colloid as it contains more particles larger than 10 nm.

Because of their outstanding properties, in the rest of the paper, we focus our attention in the CQDs synthesized with the flow jet. Figure S6 shows the UV−visible absorption spectra of CQDs, where it is possible to observe a strong absorption peak located at 220 nm, commonly associated with the transition $\pi-\pi^*$ of aromatic C−C bonds present in the CQD systems according to a bandgap transition mechanism based on conjugated π-domains.[37] It is also possible to observe that the second peak is a bit mitigated and located at 340 nm, which is related to the $n-\pi^*$ transitions due to the C═O bonds in the nanoparticle surface. Peaks at 320, 300, and 287 nm from other transitions are also observed, which might be associated to a consequence of surface passivation by the interaction between CQDs and PEG.[38] The absorption mechanism could also be explained based on the quantum-confinement effect, emissive traps located at the surface of CQDs, and radiative recombination of excitons, among others.[39] However, the aim of the present research work is not centered on elucidating the reasons behind the absorption behavior of CQDs.

On the other hand, the broadband emission photoluminescence spectra[40] of the CQDs synthesized by the flow jet strategy are shown in Figure 2c. The figure clearly illustrates that by progressively increasing the excitation wavelength from 210 to 450 nm, the fluorescence response can be tuned. The fluorescence emission peaks related to the excitation wavelengths around 287 nm are the strongest and by exciting with 280 nm, an emission peak at 376 nm with a fwhm of 77 nm is obtained. Exciting the sample with wavelengths close to 300 nm, the fluorescence obtained is reduced to 43% of the maximum and is lower when the excitation wavelengths are in the 320 nm region, 36%. This reduction implies a different mechanism of photoluminescence related to each absorption peak, leading to its association with different transitions. Fluorescence excited at 405 nm is also important as is a common excitation laser diode source for fluorescence microscope imaging applications. The fluorescence maximum obtained by exciting with 405 nm is located at 464 nm with a fwhm of 112 nm and a fluorescence emission which is 5% of the maximum emission obtained. Even though the fluorescence response gets reduced compared to 280 nm excitation, it is perfectly suitable for fluorescence imaging applications as shown in Figure 4. Besides, the increased width of the fluorescence response, together with the wide range of fluorescence excitation wavelengths, opens up the opportunity of using the generated CQDs for acquiring fluorescence images with a wide variety of detectors and excitation sources.

The Fourier-transform infrared spectroscopy (FTIR) spectra of the CQDs and PEG200 in Figure 3a exhibit the presence of new bounds generated around the CQDs. The absorption peak observed at 1646 cm^{-1} indicates the formation of C═O in the outer surface of the CQDs. The increased absorption from

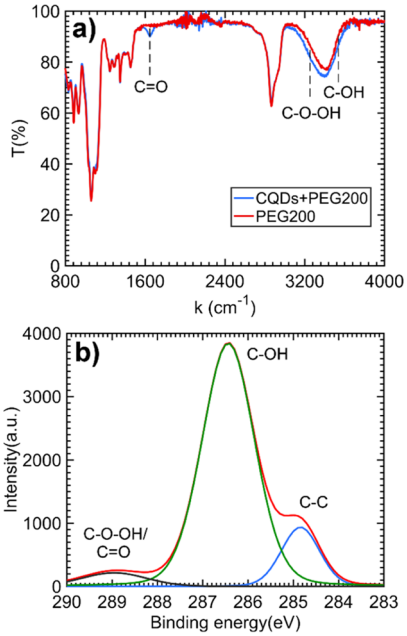

Figure 3. (a) FTIR spectra of pure PEG200 and PEG200 with CQDs. (b) XPS C 1s spectra of CQDs. The CQDs samples was the one synthesized with the flow jet processing system.

DOI: 10.1021/acsomega.7b02082
ACS Omega 2018, 3, 2735−2742

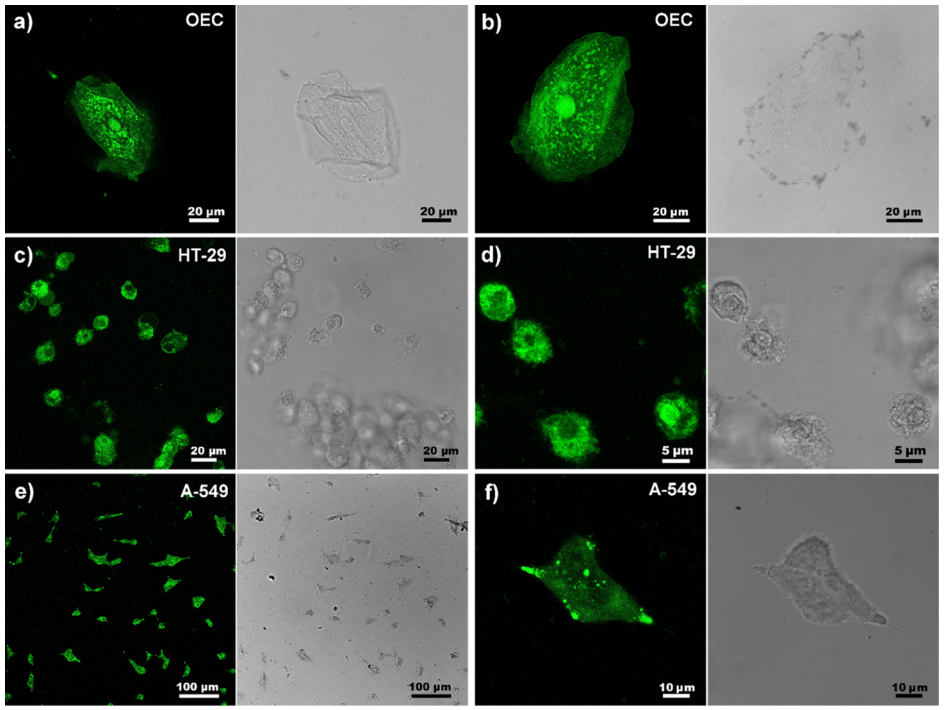

Figure 4. Confocal microscope images of different cell types, incubated with CQDs. Fluorescence images, under 405 nm for wavelength excitation, are shown on the left side and the corresponding bright-field images on the right one. (a) OEC, after 1 min of incubation at room temperature. (b) OEC, after 10 days in the microscope slide at room temperature. (c,d) Colon cancer cell line HT29, incubated at room temperature during 10 min. (e,f) Lung cancer cell line A549, incubated at room temperature during 10 min.

3000 to 3600 cm^{-1} is due to the contribution of the C−OH bond and the carboxylic group C−O−OH anchored at the nanoparticle surface.[41] The attachment of functional groups to the CQD surface was also analyzed by X-ray photoelectron spectroscopy (XPS). In Figure 3b, the analysis of the flow jet sample is shown. The overall C 1s peak in the range of 283−291 eV is fitted by a superposition of three peaks. The first binding-energy peak (284.8 eV) can be attributed to the C−C bond, whereas the other two peaks can be assigned to C−OH (286.5 eV) and C−O−OH or C═O (289.2 eV). The large C−OH peak indicates that most of surface carbon atoms are passivated through the −OH bonding. The C−C peak describes the presence of surface carbon atoms completely connected with the inner carbon atoms. The last peak is associated to carbon atoms passivated through C−O−OH or C═O bonding. The atomic concentration of functionalized carbon atoms was quantitatively evaluated based on the peak area ratios and obtained to be of approximately 85%. Because of the small size of the CQDs, the surface-area-to-volume ratio is high, approximately 1 nm^{-1}; hence, an elevated percentage of the carbon atoms is in the surface of the nanoparticle. These active carbon atoms play a very significant role in the photoluminescence of the CQDs.

CQDs have attracted widespread attention in recent years in the field of fluorescence imaging.[42,43] Here, we explore the CQDs obtained with our method for fluorescence labeling of human life cells. Three different types of cells were used: healthy oral epithelial cells (OECs) from volunteers, a lung cancer cell line A549, and a colon cancer cells line HT29. These epithelial cells are transparent and no auto-fluorescence was observed at the excitation wavelength of 405 nm while collecting the emission at 420−637 nm. Consequently, there is a need to use markers to differentiate the main organelles of the cell.

OECs were donated by 10 different healthy subjects. The samples were extracted from each subject by mechanical exfoliation accordingly to a variation of the protocol reported by Cepeda-Pérez.[44] The same protocol was followed to extract all the OECs; after the subject has rinsed the mouth using ultrapure Milli-Q water, an interdental brush was used to carefully scrape the inner area of each cheek. The scraped area was located between the first and the second molar on both sides of the jaw. A sample was taken from each individual and dispersed in 1 mL of sodium chloride solution (Fluirespira 0.9% NaCl in H_2O). It was mixed with 40 μL of CQDs dispersed in PEG200. After 1 min of incubation at room temperature a drop of the product was deposited in a microscope slide. Next, the fluorescence emission under 405 nm excitation wavelength while collecting the emission at 420−637 nm was detected by means of a confocal microscope (Leica TCS SP8). In Figure 4a, where both transmission and fluorescence images are displayed, it is shown that the CQDs enhance the morphologies of the OECs as they are well spread all over the cell with a high predominance in the nucleus. The samples of all volunteers were observed with the microscope showing similar results (see Figure S7 of Supporting Information) and a 3D image of a group of cells is represented in Supporting Information Video S2 to prove the internalization of the CQDs in the whole volume of the cell and that 3D information of the cell structures can be extracted. The image of an OEC after 10 days in the microscope slide at room temperature is shown in Figure 4b. In this case, the transmission image shows signals of cell death as lack of nuclei and membrane disruption. However, the fluorescence image shows a "frozen" image of the live cell. Therefore, this technique can be used to keep the cell

DOI: 10.1021/acsomega.7b02082
ACS Omega 2018, 3, 2735−2742

information for prolonged periods of time as the CQDs are not degraded under this circumstance.

Two different human cancer cell lines were used to test the CQDs in vitro: lung adenocarcinoma (A-549) and colon adenocarcinoma (HT-29). Cells were cultivated in DMEM high glucose supplemented with 10% fetal bovine serum, 1% L-glutamine, 1% penicillin/streptomycin, and 1% amphoterycin at 37 °C in a humidified atmosphere with 5% CO_2. 100 000 cells/well were grown on glass coverslips in a six-well plate for 24 h. Then, 40 μL/well of CQDs in PEG200 were added to the cell medium, and after 10 min at room temperature, cells were washed with Dulbecco's phosphate buffered saline (DPBS). The coverslips were placed on a microscope slide and observed under the confocal microscope. As shown in Figure 4c,d, the CQDs are completely internalized, lightening the whole cell and without any background fluorescence signal. The fluorescence of CQDs was detectable inside the cell, including nuclei, after 10 min from the addition. For HT-29, not all the nuclei contain a high concentration of CQDs; measurements for longer incubation times for HT-29, A-549, and OECs proved that nuclei internalization remains the same as that observed after 10 min incubation. This indicates that the internalization process is very fast, even faster than the time required for sample preparation. The differential factors are the cell morphology and cell structure, leading to a lower internalization in all nuclei for HT-29 (Figure 4c,d) and high nuclear internalization for OECs (Figure 4a,b, for more examples, see Figure S7, Supporting Information) and A-549 (Figure 4e,f). Please note that despite the different kind of epithelial cells, in all cases, a fluorescence image with no background is obtained, which indicates that the fabricated CQDs are clearly internalized. In the case of HT-29 (Figure 4c,d), it can be observed that CQDs accumulate at both reticular and vesicular structures in the cell, whereas in the case of A-549 (Figure 4e,f), the accumulation at vesicular structures predominates. The presence of PEG200 in the CQDs dilution helps to preserve the samples from degradation and to retain the morphology of the cells.

The integrated photostability of the CQDs during internalization in a live cell was measured, which provides a good knowledge of the CQD response for both in vivo and in vitro applications. During 5 h, the temporal evolution of the fluorescence image of a lung cancer cell, A549, irradiated with a 405 nm laser source is measured by taking an image every 20 s. The normalized photoluminescence intensity was determined by integrating the intensity value of every pixel in a defined squared area around the cell, dotted lines in Figure 5, for each image acquired during the 5 h. Then, normalization is done with respect to the value of the image with the highest integrated fluorescence. The variation of the integrated photoluminescence intensity is represented in Figure 5 together with an image of the A549 cell. It remains almost constant during 2 h and is only reduced a 40% in 5 h (see Video S3 of the Supporting Information). Conventionally widely used commercial fluorescence markers such as Alexa Fluor 488 or Alexa Fluor 568 experience the same reduction in shorter periods of time, 7[45] and 4 min,[46] respectively. As the measurements are directly performed in the cell with the confocal microscope, the decrease after 2 h of irradiation is not only due to the decay of the fluorescence of the CQDs but also due to other factors as the laser and mechanical stability of the microscope and cell movement.

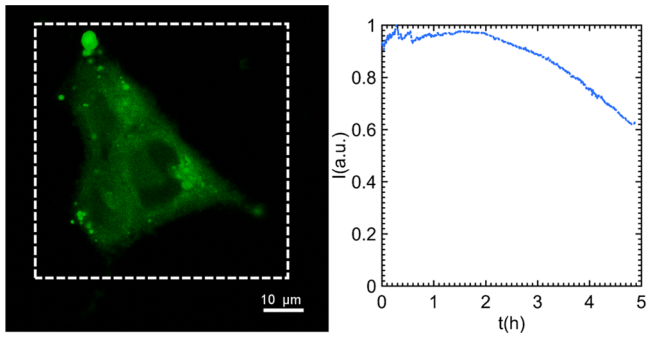

Figure 5. The temporal evolution of integrated photoluminescence intensity of the image of a lung cancer cell A549. An image at the end of 5 h of irradiation is shown on the left with the area where the intensity is integrated marked with a dotted line.

CONCLUSIONS

We developed a system for the fabrication of CQDs in PEG200 by laser irradiation based on a continuous flow jet. After 4 h of laser irradiation, the production of CQDs is higher and exhibits a smaller size than with a batch processing configuration. These facts indicate that the laser energy is more efficiently delivered to the sample thanks to the lack of losses in scattering, absorption, and its better distribution in all the volume of the liquid. Consequently, this proof-of-concept experiment gives enough evidence enforcing the statement that a system based on a continuous flow jet provides a better strategy for scaling-up the process of fabrication of CQDs from carbonaceous suspensions by laser. A study of the photoluminescence shows that CQDs exhibited an excitation-dependent emission behavior, with longer emission wavelength for longer excitation wavelength. The fluorescence emission intensity related to excitation wavelengths close to 287 nm is the strongest. A study of the surface functional groups by XPS and FTIR demonstrates the presence of C═O, C−OH, C−O−C, and C−O−OH groups which have a great potential for biological applications in conjugating drug or targeting moieties. The CQDs have been directly applied in imaging of different kinds of in vitro human cells. This study provides two important conclusions. First, the CQDs in PEG200 are a good instrument to preserve the cell information even after its death as they are not degraded and its position is kept constant. Second, a real time measurement of the integrated photostability in the cells demonstrates that the CQDs do not experience photoblinking and have a reduced photobleaching compared to standard fluorescence markers. The proposed method has a high potential for fabricating novel carbon luminescent materials by pulsed lasers radiation that can benefit many fields, such as optoelectronic, biosensing, or bioimaging.

METHODS

Materials. The flow jet experimental setup consists of simple cost-effective elements, a silicon tube, two pipette tips, and a funnel to make the liquid flow in a closed loop boosted by a peristaltic pump (Watson Marlow 313S). A picture showing the distribution of the elements can be seen in Figure S1. One of the pipette tips is cut and inserted in the other to avoid the splash of the liquid in the irradiation zone. The irradiated colloid is composed of 40 mg of carbon glassy particles dispersed in 100 mL of polyethylene glycol 200. The original size of carbon solid particles is 2−12 μm. A ball mill is used during 5 h at 300 rpm to reduce the particle size.

DOI: 10.1021/acsomega.7b02082
ACS Omega 2018, 3, 2735−2742

Theoretical Calculation. Particle heating−melting−evaporation model[24,33] was applied to estimate the necessary level of laser fluence.

Fluorescence Measurements. Fluorescence spectra shown in Figure 2c were recorded using a Cary Eclipse Fluorescence Spectrophotometer (Varian) with excitation wavelengths from 200 to 400 nm and a 10 mm path length quartz cuvette.

Infrared Spectroscopy Spectrum. The FTIR spectrum (Figure 3a) was measured using a FT/IR-6200 (Jasco) Fourier transform infrared spectrometer.

Internalization and Fluorescence Images. The samples extraction protocol is a variation of the Cepeda-Pérez.[44] The internalization of the CQDs into samples of OECs taken from 10 different subjects was analyzed by fluorescence images acquired with an inverted confocal microscope Leica TCS SP8 using a 405 nm diode as the excitation source and a PMT (photomultiplier tube) collecting light in the 420−637 nm region as the detector.

■ ASSOCIATED CONTENT

Supporting Information

The Supporting Information is available free of charge on the ACS Publications website at DOI: 10.1021/acsomega.7b02082.

(1) Experimental setup and materials and methods, (2) theoretical calculation, (3) TGA, (4) temporal evolution measurements, (5) optical properties, (6) internalization of CQDs in human cells, and (7) long-term CQDs properties (PDF)

Real-time operation of the experimental setup (AVI)

3D image of an OEC (AVI)

Photobleaching measurement of an in vitro A549 cell (AVI)

■ AUTHOR INFORMATION

Corresponding Authors

*E-mail: cdonate@uji.es (C.D.-B.).

*E-mail: gminguez@uji.es (G.M.-V.).

ORCID

Carlos Doñate-Buendia: 0000-0002-7022-0960

Author Contributions

A.P. made the theoretical model and XPS measurements. C.D.-B. synthesized the CQDs and characterized them by TEM, FTIR, UV−vis absorption, dynamic light scattering, TGA, fluorescence and QY measurements with the help of R.T.-M., M.F.-A., and G.M.-V. The biological samples were prepared and internalization results analyzed by E.F. The internalization procedure of the CQDs in biological samples and the acquisition of fluorescence and photobleaching images were done by C.D.-B. and R.T.-M. with the help of M.F.-A. and G.M.-V. All the authors contributed to the discussion of the paper and approved the manuscript. G.M.-V. and M.F.-A. directed the project.

Funding

The authors thank Generalitat Valenciana for the financial support through projects PROMETEU/2016/079 and AICO/2016/036, the University Jaume I through the project UJI B2016-19, the Ministerio de Economía y Competitividad (MINECO) through the project FIS2016-75618-R, and the Ministry of Education, Youth and Sports from the Czech Republic, in the framework of the targeted support of the "National Programme for Sustainability I" LO 1201.

Notes

The authors declare no competing financial interest.

■ ACKNOWLEDGMENTS

The authors are also very grateful to the Serveis Centrals d'Instrumentación Científica (SCIC) of the University Jaume I for the use of the femtosecond laser and microscopy facilities.

■ ABBREVIATIONS

CQDs, carbon quantum dots; fwhm, full width at half maximum; PEG, polyethylene glycol; PEG200, polyethylene glycol 200; TEM, transmission electron microscopy; TGA, thermogravimetric analysis; QY, quantum yield; UV, ultraviolet; FTIR, Fourier-transform infrared spectroscopy; XPS, X-ray photoelectron spectroscopy; OECs, oral epithelial cells; DMEM, Dulbecco's modified Eagle medium; DPBS, Dulbecco's phosphate buffered

■ REFERENCES

(1) Sun, Y.-P.; Zhou, B.; Lin, Y.; Wang, W.; Fernando, K. A. S.; Pathak, P.; Meziani, M. J.; Harruff, B. A.; Wang, X.; Wang, H.; Luo, P. G.; Yang, H.; Kose, M. E.; Chen, B.; Veca, L. M.; Xie, S.-Y. Quantum-Sized Carbon Dots for Bright and Colorful Photoluminescence. *J. Am. Chem. Soc.* **2006**, *128*, 7756−7757.

(2) Kong, B.; Zhu, A.; Ding, C.; Zhao, X.; Li, B.; Tian, Y. Carbon Dot-Based Inorganic−Organic Nanosystem for Two-Photon Imaging and Biosensing of pH Variation in Living Cells and Tissues. *Adv. Mater.* **2012**, *24*, 5844−5848.

(3) Hola, K.; Zhang, Y.; Wang, Y.; Giannelis, E. P.; Zboril, R.; Rogach, A. L. Carbon Dots—Emerging Light Emitters for Bioimaging, Cancer Therapy and Optoelectronics. *Nano Today* **2014**, *9*, 590−603.

(4) Dai, H.; Shi, Y.; Wang, Y.; Sun, Y.; Hu, J.; Ni, P.; Li, Z. A Carbon Dot Based Biosensor for Melamine Detection by Fluorescence Resonance Energy Transfer. *Sens. Actuators, B* **2014**, *202*, 201−208.

(5) Xie, C.; Nie, B.; Zeng, L.; Liang, F.-X.; Wang, M.-Z.; Luo, L.; Feng, M.; Yu, Y.; Wu, C.-Y.; Wu, Y.; Yu, S.-H. Core-Shell Heterojunction of Silicon Nanowire Arrays and Carbon Quantum Dots for Photovoltaic Devices and Self-Driven Photodetectors. *ACS Nano* **2014**, *8*, 4015−4022.

(6) Li, H.; Kang, Z.; Liu, Y.; Lee, S.-T. Carbon Nanodots: Synthesis, Properties and Applications. *J. Mater. Chem.* **2012**, *22*, 24230.

(7) Zheng, X. T.; Ananthanarayanan, A.; Luo, K. Q.; Chen, P. Glowing Graphene Quantum Dots and Carbon Dots: Properties, Syntheses, and Biological Applications. *Small* **2015**, *11*, 1620−1636.

(8) Yuan, F.; Li, S.; Fan, Z.; Meng, X.; Fan, L.; Yang, S. Shining Carbon Dots: Synthesis and Biomedical and Optoelectronic Applications. *Nano Today* **2016**, *11*, 565−586.

(9) Roy, P.; Chen, P.-C.; Periasamy, A. P.; Chen, Y.-N.; Chang, H.-T. Photoluminescent Carbon Nanodots: Synthesis, Physicochemical Properties and Analytical Applications. *Mater. Today* **2015**, *18*, 447−458.

(10) Liu, H.; Ye, T.; Mao, C. Fluorescent Carbon Nanoparticles Derived from Candle Soot. *Angew. Chem., Int. Ed.* **2007**, *46*, 6473−6475.

(11) Sahu, S.; Behera, B.; Maiti, T. K.; Mohapatra, S. Simple One-Step Synthesis of Highly Luminescent Carbon Dots from Orange Juice: Application as Excellent Bio-Imaging Agents. *Chem. Commun.* **2012**, *48*, 8835.

(12) Wang, X.; Qu, K.; Xu, B.; Ren, J.; Qu, X. Microwave Assisted One-Step Green Synthesis of Cell-Permeable Multicolor Photoluminescent Carbon Dots without Surface Passivation Reagents. *J. Mater. Chem.* **2011**, *21*, 2445.

(13) Lai, C.-W.; Hsiao, Y.-H.; Peng, Y.-K.; Chou, P.-T. Facile Synthesis of Highly Emissive Carbon Dots from Pyrolysis of Glycerol;

DOI: 10.1021/acsomega.7b02082
ACS Omega 2018, 3, 2735−2742

Gram Scale Production of Carbon dots/mSiO$_2$ for Cell Imaging and Drug Release. *J. Mater. Chem.* **2012**, *22*, 14403.
(14) Ma, Z.; Ming, H.; Huang, H.; Liu, Y.; Kang, Z. One-Step Ultrasonic Synthesis of Fluorescent N-Doped Carbon Dots from Glucose and Their Visible-Light Sensitive Photocatalytic Ability. *New J. Chem.* **2012**, *36*, 861−864.
(15) Reyes, D.; Camacho, M.; Camacho, M.; Mayorga, M.; Weathers, D.; Salamo, G.; Wang, Z.; Neogi, A. Laser Ablated Carbon Nanodots for Light Emission. *Nanoscale Res. Lett.* **2016**, *11*, 424.
(16) Tarasenka, N.; Stupak, A.; Tarasenko, N.; Chakrabarti, S.; Mariotti, D. Structure and Optical Properties of Carbon Nanoparticles Generated by Laser Treatment of Graphite in Liquid. *ChemPhysChem* **2017**, *18*, 1074−1083.
(17) Li, X.; Wang, H.; Shimizu, Y.; Pyatenko, A.; Kawaguchi, K.; Koshizaki, N. Preparation of Carbon Quantum Dots with Tunable Photoluminescence by Rapid Laser Passivation in Ordinary Organic Solvents. *Chem. Commun.* **2011**, *47*, 932−934.
(18) Nguyen, V.; Yan, L.; Si, J.; Hou, X. Femtosecond Laser-Induced Size Reduction of Carbon Nanodots in Solution: Effect of Laser Fluence, Spot Size, and Irradiation Time. *J. Appl. Phys.* **2015**, *117*, 084304.
(19) Hu, S.-L.; Niu, K.-Y.; Sun, J.; Yang, J.; Zhao, N.-Q.; Du, X.-W. One-Step Synthesis of Fluorescent Carbon Nanoparticles by Laser Irradiation. *J. Mater. Chem.* **2009**, *19*, 484−488.
(20) Amans, D.; Chenus, A.-C.; Ledoux, G.; Dujardin, C.; Reynaud, C.; Sublemontier, O.; Masenelli-Varlot, K.; Guillois, O. Nanodiamond Synthesis by Pulsed Laser Ablation in Liquids. *Diam. Relat. Mater.* **2009**, *18*, 177−180.
(21) Yang, L.; May, P. W.; Yin, L.; Smith, J. A.; Rosser, K. N. Growth of Diamond Nanocrystals by Pulsed Laser Ablation of Graphite in Liquid. *Diam. Relat. Mater.* **2007**, *16*, 725−729.
(22) Cao, L.; Wang, X.; Meziani, M. J.; Lu, F.; Wang, H.; Luo, P. G.; Lin, Y.; Harruff, B. a.; Veca, L. M.; Murray, D.; Xie, S.-Y.; Sun, Y.-P. Carbon Dots for Multiphoton Bioimaging. *J. Am. Chem. Soc.* **2007**, *129*, 11318−11319.
(23) Yang, S.-T.; Cao, L.; Luo, P. G.; Lu, F.; Wang, X.; Wang, H.; Meziani, M. J.; Liu, Y.; Qi, G.; Sun, Y.-P. Carbon Dots for Optical Imaging in Vivo. *J. Am. Chem. Soc.* **2009**, *131*, 11308−11309.
(24) Pyatenko, A.; Wang, H.; Koshizaki, N.; Tsuji, T. Mechanism of Pulse Laser Interaction with Colloidal Nanoparticles. *Laser Photonics Rev.* **2013**, *7*, 596−604.
(25) Xiao, J.; Liu, P.; Wang, C. X.; Yang, G. W. External Field-Assisted Laser Ablation in Liquid: An Efficient Strategy for Nanocrystal Synthesis and Nanostructure Assembly. *Prog. Mater. Sci.* **2017**, *87*, 140−220.
(26) Zhang, D.; Gökce, B.; Barcikowski, S. Laser Synthesis and Processing of Colloids: Fundamentals and Applications. *Chem. Rev.* **2017**, *117*, 3990−4103.
(27) Maximova, K.; Aristov, A.; Sentis, M.; Kabashin, A. V. Size-Controllable Synthesis of Bare Gold Nanoparticles by Femtosecond Laser Fragmentation in Water. *Nanotechnology* **2015**, *26*, 065601.
(28) González-Rubio, G.; Guerrero-Martínez, A.; Liz-Marzán, L.-M. Reshaping, Fragmentation, and Assembly of Gold Nanoparticles Assisted by Pulse Lasers. *Acc. Chem. Res.* **2016**, *49*, 678−686.
(29) González-Rubio, G.; Díaz-Núñez, P.; Rivera, A.; Prada, A.; Tardajos, G.; González-Izquierdo, J.; Bañares, L.; Llombart, P.; Macdowell, L. G.; Palafox, M. A.; Palafox, M. A.; Liz-Marzán, L. M.; Peña-Rodríguez, O.; Guerrero-Martínez, A. Femtosecond Laser Reshaping Yields Gold Nanorods with Ultranarrow Surface Plasmon Resonances. *Science* **2017**, *358*, 640−644.
(30) Wagener, P.; Barcikowski, S. Laser Fragmentation of Organic Microparticles into Colloidal Nanoparticles in a Free Liquid Jet. *Appl. Phys. A* **2010**, *101*, 435−439.
(31) Kuzmin, P. G.; Shafeev, G. A.; Serkov, A. A.; Kirichenko, N. A.; Shcherbina, M. E. Laser-Assisted Fragmentation of Al Particles Suspended in Liquid. *Appl. Surf. Sci.* **2014**, *294*, 15−19.
(32) Lau, M.; Barcikowski, S. Quantification of Mass-Specific Laser Energy Input Converted into Particle Properties during Picosecond Pulsed Laser Fragmentation of Zinc Oxide and Boron Carbide in Liquids. *Appl. Surf. Sci.* **2015**, *348*, 22−29.
(33) Pyatenko, A.; Yamaguchi, M.; Suzuki, M. Mechanisms of Size Reduction of Colloidal Silver and Gold Nanoparticles Irradiated by Nd:YAG Laser. *J. Phys. Chem. C* **2009**, *113*, 9078−9085.
(34) Palik, E. D. *Handbook of Optical Constants of Solids*; Academic Press: New York, 1998; Vol. 3, p 999.
(35) Chase, M. W.; Curnutt, J. L.; Hu, A. T.; Prophet, H.; Syverud, A. N.; Walker, L. C. JANAF Thermochemical Tables, 1974 Supplement. *J. Phys. Chem. Ref. Data* **1974**, *3*, 311−480.
(36) Allen, M. W. *Measurement of Fluorescence Quantum Yields*; Technical Note: 52019; Thermo Fisher Scientific: Madison, WI, USA, 2010; pp 1−4.
(37) Wang, Y.; Kalytchuk, S.; Zhang, Y.; Shi, H.; Kershaw, S. V.; Rogach, A. L. Thickness-Dependent Full-Color Emission Tunability in a Flexible Carbon Dot Ionogel. *J. Phys. Chem. Lett.* **2014**, *5*, 1412−1420.
(38) Zhu, S.; Shao, J.; Song, Y.; Zhao, X.; Du, J.; Wang, L.; Wang, H.; Zhang, K.; Zhang, J.; Yang, B. Investigating the surface state of graphene quantum dots. *Nanoscale* **2015**, *7*, 7927−7933.
(39) Zhu, S.; Song, Y.; Zhao, X.; Shao, J.; Zhang, J.; Yang, B. The photoluminescence mechanism in carbon dots (graphene quantum dots, carbon nanodots and polymer dots): current state and future perspective. *Nano Res.* **2015**, *8*, 355−381.
(40) Khan, S.; Gupta, A.; Verma, N. C.; Nandi, C. K. Time-Resolved Emission Reveals Ensemble of Emissive States as the Origin of Multicolor Fluorescence in Carbon Dots. *Nano Lett.* **2015**, *15*, 8300−8305.
(41) Socrates, G. *Infrared and Raman Characteristic Group Frequencies: Tables and Charts*, 3rd ed.; John Wiley & Sons, 2001; p 347.
(42) Luo, P. G.; Yang, F.; Yang, S.-T.; Sonkar, S. K.; Yang, L.; Broglie, J. J.; Liu, Y.; Sun, Y.-P. Carbon-Based Quantum Dots for Fluorescence Imaging of Cells and Tissues. *RSC Adv.* **2014**, *4*, 10791−10807.
(43) Liu, Q.; Guo, B.; Rao, Z.; Zhang, B.; Gong, J. R. Strong Two-Photon-Induced Fluorescence from Photostable, Biocompatible Nitrogen-Doped Graphene Quantum Dots for Cellular and Deep-Tissue Imaging. *Nano Lett.* **2013**, *13*, 2436−2441.
(44) Cepeda-Pérez, E.; López-Luke, T.; Plascencia-Villa, G.; Perez-Mayen, L.; Ceja-Fdez, A.; Ponce, A.; Vivero-Escoto, J.; de la Rosa, E. SERS and Integrative Imaging upon Internalization of Quantum Dots into Human Oral Epithelial Cells. *J. Biophot.* **2016**, *9*, 683−693.
(45) Hayashi-Takanaka, Y.; Stasevich, T. J.; Kurumizaka, H.; Nozaki, N.; Kimura, H. Evaluation of Chemical Fluorescent Dyes as a Protein Conjugation Partner for Live Cell Imaging. *PLoS One* **2014**, *9*, e106271.
(46) Mahmoudian, J.; Hadavi, R.; Jeddi-Tehrani, M.; Mahmoudi, A. R.; Bayat, A. A.; Shaban, E.; Vafakhah, M.; Darzi, M.; Tarahomi, M.; Ghods, R. Comparison of the Photobleaching and Photostability Traits of Alexa Fluor 568- and Fluorescein Isothiocyanate-Conjugated Antibody. *Cell J.* **2011**, *13*, 169−172.

DOI: 10.1021/acsomega.7b02082
ACS Omega 2018, 3, 2735−2742